

# Molecular Dynamics Simulations of Two Tandem Octarepeats from the Mammalian Prion Protein: Fully $\text{Cu}^{2+}$ -bound and Metal-Free Forms

M. Jake Pushie and Hans J. Vogel

Structural Biology Research Group, Department of Biological Sciences, University of Calgary, Calgary, Alberta, Canada

**ABSTRACT** Molecular dynamics simulations have been conducted on a model fragment ( $\text{Ac-PHGGGWGQPHGGGW-NH}_2$ ) of the prion protein octarepeat domain, both in the  $\text{Cu}^{2+}$ -bound and metal-free forms. The copper-bound models are based on the consensus structure of the core  $\text{Cu}^{2+}$ -binding site of an individual octarepeat, relevant to the fully  $\text{Cu}^{2+}$ -occupied prion protein octarepeat region. The model peptides contain  $\text{Cu}^{2+}$  bound through a His imidazole ring and two deprotonated amide N-atoms in the peptide backbone supplied by the following two Gly residues. Both the copper-bound and metal-free models have been simulated with the OPLS all-atom force field with the GROMACS molecular dynamics package. These simulations, with two tandem copper-binding sites, represent the minimum model necessary to observe potential structuring between the copper-binding sites in the octarepeat region. The GWGQ residues constitute a flexible linker region that predominantly adopts a turn, serving to bring adjacent His residues into close proximity. The consequent formation of stable structures demonstrates that the copper-bound octarepeat region allows the copper-coordinating sites to come into van der Waals contact, packing into particular orientations to further stabilize the bend in the GWGQ linker region.

## INTRODUCTION

The prion protein (PrP) is a C-terminal glycosylphosphatidylinositol-anchored cell-surface protein that is implicated as the causative agent in transmissible neurological conditions such as Creutzfeldt-Jakob disease in humans, chronic wasting disease in deer and elk, and bovine spongiform encephalopathy, more commonly known as mad cow disease (1). The protein contains 208 amino acid residues and a single disulfide bond, and has two oligosaccharides attached (1). Although residues 120–208 of the C-terminal domain are structured, the N-terminal domain has been shown to be flexible and disordered in aqueous solution (2–4). The infectious form of PrP arises, via an as-yet enigmatic conformational misfolding process, from its native form, which is relatively high in  $\alpha$ -helical character (5), to a conformation with increased  $\beta$ -sheet content. These misfolded molecules can aggregate, resulting in fibril formation, which in turn influences other PrP molecules to misfold and aggregate. The PrP aggregates are known to be protease-resistant (6), but the N-terminal region is not, and it is usually absent in the mature PrP aggregates.

The biological function of PrP is not yet fully understood and although it is expressed in most tissues, the highest concentration is found at the surface of the synapse. In humans, the flexible N-terminal domain contains four tandem copper-binding repeats, each containing eight amino acids, with the sequence  $(\text{PHGGGWGQ})_4$ , termed the octarepeat (OR) region, shown in Fig. 1 A. Although the number of

repeats varies among mammals, the sequence of an individual OR is highly conserved across virtually all mammalian species (7), and each domain has a high specificity for binding  $\text{Cu}^{2+}$  over other divalent metal ions (8–11).

Copper is used by neurons for signaling, and the cellular form of PrP appears to be finely tuned to bind  $\text{Cu}^{2+}$  within the concentration range found at the synaptic junction (12). There have been strong suggestions that the native form of PrP may function to buffer the copper concentration at the synapse (13). Within biological systems, the availability and transfer of copper is tightly regulated, where the concentration of free cytoplasmic  $\text{Cu}^{2+}$  is on the order of less than one atom per cell (14). Organisms have evolved tight control mechanisms over copper transport and utilization, because free copper readily initiates reactions that in aqueous environments generate reactive oxygen species (ROS), such as highly reactive hydroxyl radicals (15). The mechanisms by which ROS may be generated by  $\text{Cu}^{2+}$  are the Haber-Weiss (16) and Fenton-type (reviewed in (17)) mechanisms, which have been extensively characterized. Because of its environmental specificity for  $\text{Cu}^{2+}$ , it has been proposed that PrP is a  $\text{Cu}^{2+}$  transporter or chaperone (18) and may also have a role in protecting the synapse from the deleterious effects of ROS generation by excesses of copper released from neurons.

Copper binding to the OR region of PrP has been demonstrated to confer proteinase-K resistance to this region of PrP (19). The connection between the involvement of copper and prion disease is not clear-cut, as mice treated with a  $\text{Cu}^{2+}$ -specific chelator (D-penicillamine) demonstrated a delayed onset of disease (20). Although the N-terminal portion of PrP has been shown to be proteolytically removed in the protease-resistant form (21), there is evidence that individuals with

*Submitted March 23, 2007, and accepted for publication July 11, 2007.*

Address reprint requests to Hans J. Vogel, Dept. of Biological Sciences, University of Calgary, 2500 University Dr. NW, Calgary, Alberta, T2N 1N4, Canada. Tel.: 403-220-6006; Fax: 403-289-9311; E-mail: vogel@ucalgary.ca.

Editor: Ruth Nussinov.

© 2007 by the Biophysical Society  
0006-3495/07/12/3762/13 \$2.00

doi: 10.1529/biophysj.107.109512

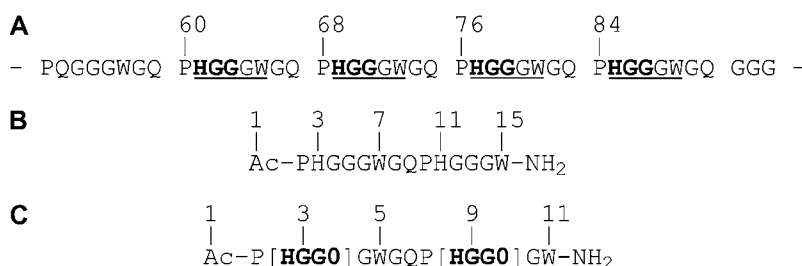


**FIGURE 1** (A) The octarepeat region of the prion protein, spanning residues 60–91 (human numbering). Underlined residues are required for reproducing the spectral fingerprint of copper binding to the full-length prion protein; bold-face residues constitute the core copper-binding environment. (B) Metal-free OR<sub>2</sub> model. (C) Metal-bound OR<sub>2</sub> model with new copper-containing residue type shown in square brackets.

additional OR sites, arising from spontaneous gene mutation, for example, have an increased susceptibility to prion diseases (22–25). The prevalence of OR insertion mutations in disease cases implies that such alterations are a risk factor for developing inherited prion disease (i.e., without extraneous influence from infectious PrP particles). Modification of the number of octarepeats, and its apparent predisposing of individuals to prion disease, is not the rule. Transgenic mice expressing an OR-deletion form of PrP display slowed disease progression and altered disease pathology (26).

In addition to the process of protein misfolding, disruption of metal ion homeostasis is also a hallmark of prion diseases (27), as is PrP oxidation (28). These features are not unique to prion disease, and are also observed in Alzheimer's disease, a neurodegenerative condition involving aggregation of proteinaceous material that is rich in the metal ions copper, iron, and zinc (29). Like Cu<sup>2+</sup> bound to PrP (at low Cu/PrP ratios), copper bound in Alzheimer plaques is also redox active, and oxidative damage, as well as copper-mediated ROS generation, are hallmarks of this disease (30).

Taken together, the above observations suggest that even though the ORs are not required structurally for propagating PrP misfolding, they may play a role in the development of prion disease.

The core copper-binding region of the fully Cu<sup>2+</sup>-loaded PrP ORs consists of only the HGG amino acid portion. The copper is anchored by the first imidazole-ring nitrogen, N<sub>δ</sub>1, of the His residue, and through the deprotonated amide backbone N-atoms of the two Gly residues and the carbonyl oxygen of the second Gly. The following two residues in the OR region, the third Gly and the Trp residue, facilitate in stabilizing the structure of the binding site (31). X-ray crystallographic data for a copper-bound form of the octarepeat fragment HGGGW has been reported (32).

X-ray crystallography and nuclear magnetic resonance (NMR) are the most commonly employed techniques to obtain protein structure information of atomic resolution. Due to the lack of persistent long-range structure, and the flexible nature of the N-terminal domain of PrP, this portion of the intact protein has not been amenable to crystallographic analysis, and it is often removed to aid in crystallization of PrP (33). On the other hand, Cu<sup>2+</sup> contains one unpaired electron, which increases the relaxation rate of any nearby nuclei, effectively making much of the local chemical information invisible to conventional NMR structure methods.

A significant volume of work has been done to characterize the structure of the OR region in the absence of Cu<sup>2+</sup>. Although the flexibility of the N-terminal repeat region of mammalian PrP has been confirmed by structure methods such as circular dichroism (CD) (34–36) and NMR (37–40), these same experiments show evidence of transient secondary structure within the OR region. For example, NMR experiments by Yoshida et al. (39) and Zahn (40) suggested that the GWGQ region can transiently adopt a  $\beta$ -turn, whereas the HGGGW region adopts a loop structure with the His imidazole and Trp indole rings in close proximity. Based on fluorescence quenching measurements, Gustiananda et al. suggested that either a protonated or neutral imidazole ring may be able to participate in stabilizing a loosely folded structure through cation- $\pi$  or  $\pi$ - $\pi$  interactions with the indole ring of Trp (41).

Due to the experimental constraints in characterizing structural elements in the N-terminal domain in the presence of Cu<sup>2+</sup>, mentioned above, our goal has been to design a new copper-containing residue topology using high-level quantum-chemical methods. In this work, we have derived the necessary force field parameters for the unusual backbone-deprotonated and metal-coordinated HGG fragment with Cu<sup>2+</sup>, using models of the copper-binding region of the ORs based on computational studies (42), available crystallographic data (32), and donor ligands observed in electron paramagnetic resonance (EPR) results of the residues making up the binding site (43). The newly designed copper-containing model has been incorporated into a minimal model peptide fragment spanning two OR sites to analyze their structure propensity in molecular dynamics simulations. The same peptide fragment in the absence of Cu<sup>2+</sup> has also been simulated for comparison. The models used herein are models of a two-OR fragment of the mammalian prion protein in the absence of Cu<sup>2+</sup> and under full Cu<sup>2+</sup> occupancy conditions, and they represent the minimum construct necessary to observe potential interactions between adjacent N-terminal copper-bound OR sites.

## COMPUTATIONAL PROCEDURE

### Density functional theory and derivation of force field parameters

Unrestricted density functional theory (DFT) calculations were carried out at the B3LYP level of theory (44) using the Gaussian 03 (G03) suite of

programs (45). Geometry optimizations were carried out without geometry or symmetry constraints at the B3LYP/6-31G(d) level, followed by frequency calculations (keyword freq). The larger 6-311+G(2df,2p) basis set was used to obtain more accurate relative energy differences for the B3LYP/6-31G(d)-optimized structures. Solvation effects were approximated for the optimized structures using a polarizable continuum model available in G03 (SCRF = IEFPCM) using a united-atom approach with aliphatic H-atoms summed into their parent heavy-atom radii (46,47).

Geometry optimizations were used to determine the lowest energy conformations of the copper-bound peptide fragment:  $[\text{Cu}^{\text{II}}(\text{Ac-HGGG-NH}_2)_{-2\text{H}}]^0$ , as well as several smaller hydrated  $\text{Cu}^{2+}$  complexes. In the case of the polypeptide models, the capping acetyl (Ac) and  $\text{NH}_2$  groups mimic the peptide bonding found in a larger protein environment and abrogate the undesirable effects of charged termini in the model calculations. All geometries were optimized until the predicted change in energy was typically  $<0.3 \times 10^{-3} \text{ kJ mol}^{-1}$ . The energy-minimized structures have no imaginary frequencies, confirming that these structures are at a stationary point on the potential energy surface.

## Representation of $\text{Cu}(\text{HGG})_{-2\text{H}}$ in MD simulations

New copper-containing residues have been named HGG0 and HGG1. The HGG0 topology contains no water molecules explicitly coordinated to the metal center, whereas the HGG1 model (used in initial trial simulations and not shown) contains only one water molecule above the coordination plane, as is evidenced in the crystal structure (32).

Copper coordination to the HGG fragment requires removal of both of the Gly amide H-atoms. The free bond sites at the amide N-atoms are instead occupied by the central copper atom, approximately along the same bond vector that would have otherwise been occupied by an H-atom. This type of copper-binding observed within the OR region is not accounted for in any of the force fields available due to several factors: 1), the  $\text{Cu}^{2+}$ -binding Gly residues are missing their backbone H-atoms; 2), there are no implemented parameters for  $\text{Cu}^{2+}$  to dictate acceptable coordination geometries; 3), the redistributed charges on the backbone along the residues about the metal center are not represented; and 4), the  $\text{Cu}^{2+}$ -ligand force constants are not known.

Structure parameters such as bond length, angle, and dihedrals for the new copper-containing residues were assigned based on x-ray (32), and structure data from computational models (42). All bonds, angles, and improper dihedrals are restrained using a harmonic potential. The Ryckaert-Bellemans potential is used for all dihedrals across the copper-complex. Within the copper-bound HGG fragment, harmonic potentials are used for all improper angles that cross through the copper complex, to maintain the correct shape of the binding site (approximately square planar). The dihedral angle restraints include those necessary to maintain correct backbone atom placement within the coordination plane.

## Designing a $\text{Cu}^{2+}$ -containing HGG topology for OPLS

To adequately represent the copper-binding HGG portion of the OR region, its physical properties must be derived in the same manner as is used for the parent force field.

Atom-centered charges for the  $(\text{Cu}^{\text{II}}(\text{HGG})_{-2\text{H}})$  region of the binding site, with one explicitly coordinated solvent molecule, have been obtained using the CHELPG charge derivation method (48), at the B3LYP/6-31G(d) level of theory, to represent the distribution of charge density at the coordination site. The same CHELPG method was used in the determination of atom-centered charges used in the parameterization of the AMBER force field—from which the charges were derived for the OPLS force field (see below). The calculated CHELPG charges for the new copper-containing topologies are close in magnitude to those of their related atoms in the OPLS force field. Additional details of the charge model and related OPLS charges for comparison with those derived are contained in Fig. S1 in Supplementary Material.

The force constants used to represent the copper-ligand (Cu-L) bonds in the OPLS force field are determined from the output of the G03 frequency

calculations, calculated at the B3LYP/6-31G(d) level with the keyword freq. Since it is problematic to isolate vibrations due only to Cu-L stretching modes in large polydentate complexes like  $(\text{Cu}^{\text{II}}(\text{Ac-HGGG-NH}_2)_{-2\text{H}})$ , we instead analyzed the analogous bond stretching modes in model  $\text{Cu}^{2+}$  complexes containing a number of waters of hydration, as well as small molecule derivatives of the desired protein donor ligands (methylimidazole, water, and various coordination modes of N-methylacetamide). Summarized in Table 1, the OPLS force-constant parameters have been determined from the  $\nu(\text{Cu-L})$  modes of these small hydrated copper complexes, output in  $\text{mDyne } \text{\AA}^{-1}$ , and scaled by 60230 to convert them to harmonic bond force constants (in  $\text{kJ } \text{\AA}^{-2}$ ) for the OPLS force field.

The HGG0 topology includes all of the bond, angle, and dihedral restraints of the parent amino acids His and Gly. In addition to these restraints, additional angle and dihedral angle restraints are included for all possible angles that include the  $\text{Cu}^{2+}$  center. In addition to the HGG0 restraints, the HGG1 topology uses a set of restraints to maintain placement of the axial solvent molecule. A series of HGG1-containing molecules was also supplemented with a minimal set of restraints (one distance and two dihedral angles) to maintain the placement and orientation of the Trp indole side chain in the orientation observed in the crystal structure (32).

## Molecular dynamics simulations

MD simulations were carried out using GROMACS software, version 3.1.2 (49,50), with the OPLS-(AA)/L all-atom force field (51). Temperature (300 K) and pressure (1 bar) were kept constant by weakly coupling the system to an external temperature bath ( $\tau = 0.1$  for temperature, and  $\tau = 1.0$  for pressure) (52). The particle-mesh Ewald (PME) method was employed for long-range electrostatics (53). SETTLE (for water) and LINCS were used to constrain bond lengths (54,55). Simple point charge (SPC) waters, used in all of the simulations, were minimized by steepest descent ( $md = \text{steep}$ ) before simulation. All systems were equilibrated for 5 ns before production runs. All simulations employed a 2-fs time step and periodic boundary conditions. As all model peptide fragments are overall charge-neutral, no counterions were added.

The DSSP program was used for secondary structure analysis of all simulations (56). Molecular visualizations were created using VMD (57), and MOLMOL (58). The GROMACS program `g_mindist` was used to verify that the simulation box sizes were sufficiently large, such that the peptide was not affected by its reflected partners in the periodic array. Cluster analysis was performed using the `g_cluster` program, with structures generated from the molecular trajectory files every 10 ps and grouped according to their respective root mean-square deviations (RMSDs), based on the method of Daura, et al. (59).

Characterization of the structure preference and conformational dynamics of the metal-free  $\text{OR}_2$  model ( $\text{Ac-PHGGGWGQPHGGGW-NH}_2$  (Fig. 1 B)) was carried out in a  $4.5 \times 4.5 \times 4.5\text{-nm}$  box containing 2938 SPC water molecules for a simulated time of 150 ns.

Initial simulations containing a single  $\text{Cu}^{2+}$ -bound HGG site (sequence:  $\text{Ac-P[HGG0]GW-NH}_2$ ) in a  $3.0 \times 3.0 \times 3.0\text{-nm}$  box containing 857 SPC water molecules were run for 5 ns at simulated temperatures of 300 and 500 K to ensure structure stability of the core  $\text{Cu}^{2+}$ -binding region and to monitor its behavior.

Larger simulations that contain two adjacent  $\text{Cu}^{2+}$ -bound HGG fragments representing a portion of the mammalian PrP OR region are depicted in Fig. 1 C. The metal-bound  $\text{OR}_2$  simulations were carried out in a  $4.5 \times 4.5 \times 4.5\text{-nm}$  box containing 2938 SPC water molecules.

## Representation of HGG fragment models

To aid in the presentation and discussion of the copper-containing  $\text{OR}_2$  simulations, a simplified representation of the peptide fragments is used below. The following description presents the portions of the molecule necessary to orient the reader in further discussions. The N- and C-terminal ends

(CH<sub>3</sub>-C(O)- and NH<sub>2</sub>, respectively) are displayed in all such representations. The Pro residues are represented as five-member rings, whereas the copper-binding plane and indole ring are represented by flat discs of sizes that represent their actual structures. Interactions involving the copper-binding regions are described as involving the top or bottom face of the binding plane. These facial distinctions are defined with the N-terminal end (and the imidazole ring of His) on the left of the plane, and the C-terminal end on the right. These relative orientations of the copper-binding site will be used throughout. When referring to relative orientations and structuring between two copper-bound regions, the N-terminal site is noted first, collectively referred to as residue 3 in the sequence (Fig. 1 C), followed by the second C-terminal copper-bound region, residue 9 in the sequence. For example, a bottom-to-bottom stacked structure (abbreviated b→b) indicates that the bottom face of the first copper-binding site is interacting with the bottom face of the second.

# RESULTS

## DFT structure calculations of N<sub>3</sub>O<sub>1</sub>-coordinated [Cu<sup>II</sup>(Ac-HGGG-NH<sub>2</sub>)<sub>-2H</sub>]<sup>0</sup>

The most stable core N<sub>3</sub>O<sub>1</sub>-coordination geometries for seven stable conformations found for [Cu<sup>II</sup>(Ac-HGGG-NH<sub>2</sub>)<sub>-2H</sub>]<sup>0</sup>—with coordination via the histidine N<sub>δ</sub>-atom and the first two Gly amide N-atoms—differs in the relative orientation of the His side chain and backbone atoms. The published crystal structure (32) shows the C<sub>β</sub> group of His to

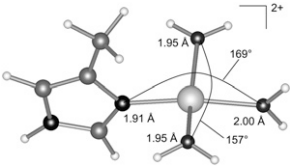
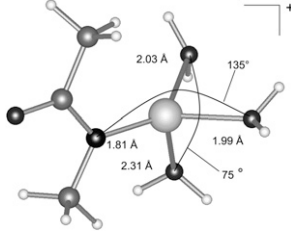
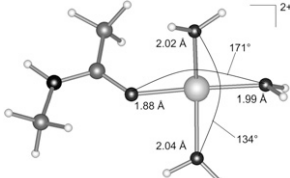
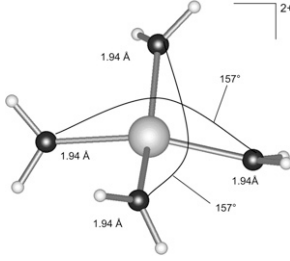
be oriented below the copper plane and the C<sub>α</sub> group above, with the imidazole ring lying approximately in the copper-peptide coordination plane. This geometry appears to be the global minimum. The nearest local minimum has the opposite orientation of the C<sub>β</sub> and C<sub>α</sub> groups and the imidazole ring is twisted out of the coordination plane. Their calculated relative energy difference (Δ*H*<sub>(g)</sub>) at the B3LYP/6-311+G(2df,2p) level is 8.64 kJ mol<sup>-1</sup>, favoring the crystal-structure-like geometry (geometry 1). Determination of the relative aqueous free energy (Δ*G*<sub>(aq)</sub> in Eq. 1) requires calculating the relative gas-phase free energy change and applying a correction for the free energy of solvation upon going from the gas phase to the solvated state (ΔΔ*G*<sub>(solv)</sub> in Eq. 1) for each species.

$$\Delta G_{(aq)} = \Delta H_{(g)} - T\Delta S_{(g)} + \Delta\Delta G_{(solv)} \quad (1)$$

Equation 2 shows the expansion of Eq. 1, with the individual terms calculated for each structure, corrected from 1 atm to 1 M concentration.

$$\begin{aligned} \Delta G_{(aq)} = & (E_{G2} - E_{G1} + 0.98(ZPE_{G2} - ZPE_{G1})) \\ & - (0.298(S_{G2}^{1M} - S_{G1}^{1M})) \\ & + (\Delta G_{(solv)G2} - \Delta G_{(solv)G1}). \end{aligned} \quad (2)$$

**TABLE 1** Small-molecule models used for the derivation of Cu-L harmonic bond force constants for OPLS

Ligand (coordinating atom)	Methylimidazole (N <sub>δ</sub> -bound)	N-methylactamide (N <sup>-</sup> -bound)
		
<i>ν</i> (Cu-L), cm <sup>-1</sup>	Cu-N <sub>δ</sub> 452	Cu-N <sup>-</sup> 479
Force constant (calc) (mDyne Å <sup>-1</sup> )	0.7485	0.2821
Harmonic potential ( <i>k</i> <sub>OPLS</sub> ) (kJ Å <sup>-2</sup> )	45082	33982*
	N-methylactamide (C(O)-bound)	Tetraaquo copper(II) (O-atom-bound)
		
<i>ν</i> (Cu-L) (cm <sup>-1</sup> )	Cu-O <sub>carbonyl</sub> 477	Cu-O <sub>water</sub> 440
Force constant (calc) (mDyne Å <sup>-1</sup> )	0.6130	0.5948
Harmonic potential ( <i>k</i> <sub>OPLS</sub> ) (kJ Å <sup>-2</sup> )	36921	35824

\*The force constant is scaled up from the calculated value due to reduced total charge of the molecule.

With these terms included, the relative stability of the crystal-structure-like geometry is further enhanced relative to geometry 2, such that the free energy difference is  $14.67 \text{ kJ mol}^{-1}$ , favoring geometry 1 (geometries 1 and 2 are shown in Figs. S2 and S3 in Supplementary Material). The relative RMSD between the HGG heavy atoms of the two calculated structures is  $0.80 \text{ \AA}$ , whereas the same difference between geometry 1 (which is similar to the crystal structure) and the published x-ray crystal structure is  $0.29 \text{ \AA}$ . Heavy-atom overlays of each of these structures are presented in Fig. S4 in Supplementary Material. Comparing the other optimized conformations to geometry 1 (whose relative energy is set to 0), their relative  $\Delta G_{(\text{aq})}$ s range from 20.68 to  $48.00 \text{ kJ mol}^{-1}$  higher in energy.

### Metal-free OR<sub>2</sub>: Ac-PHGGGWGQPHGGGW-NH<sub>2</sub>

The metal-free form of the two-octarepeat peptide fragment was run for a simulation time of 150 ns. Over the course of the entire 150-ns simulation, the GWGQ linker region frequently samples bend-and-turn-type conformations. The bend-and-turn conformations of the linker region have similar overall structure, as shown by the fit of the GWGQ backbone from structures randomly sampled from the simulation depicted in Fig. 2. The GWGQ portion, which starts fully elongated, forms a bend, as identified by secondary-structure analysis (not shown), within the first 2.5 ns of the 5-ns equilibration phase (which is not included in the 150-ns analysis). Bends do not have any specific H-bonding pattern and are defined as a direction change of  $>70^\circ$  (56). Turns are identified by specific H-bonding and are also sampled by the GWGQ region. The initial bend conformation forms a transiently stable turn from 45 to 48.2 ns with an H-bond ( $2.21 \pm 0.65 \text{ \AA}$ ) between the Gly-6 amide H-atom and the Gln-9 amide O-atom. The bend conformation continues to persist for the first 90 ns before adopting a more defined turn-type structure.

The second turn conformation forms after 90 ns and is identified by an H-bond ( $2.52 \pm 0.55 \text{ \AA}$ ) between the Gly-6 (residue  $i$  in Fig. 1 B) carbonyl O-atom and the Gln-9 (residue  $i + 4$ ) amide H-atom. The GWGQ region then interconverts between a bend and a turn. The Gly-6 amide H-atom also forms a transiently stable H-bond ( $2.58 \pm 1.18 \text{ \AA}$ ) with the amide O-atom of Gly-14 over the course of 95–150 ns. The average  $\Phi$  and  $\Psi$  angles in the linker-region turn for

residues  $i + 1$  (Trp-7) and  $i + 2$  (Gly-8) from 90 to 150 ns are  $\Phi_{i+1} = -69 \pm 17^\circ$ ,  $\Psi_{i+1} = 122 \pm 11^\circ$ ,  $\Phi_{i+2} = 120 \pm 9^\circ$ ,  $\Psi_{i+2} = -18 \pm 15^\circ$ . Plots of the  $\Phi$  and  $\Psi$  angles of these residues are displayed in Fig. S5 in Supplementary Material. These  $\Phi$  and  $\Psi$  angles appear to be most consistent with a type II  $\beta$ -turn, with the Gly residue in the  $i + 2$  position, allowing for greater flexibility. Before the 90-ns time point, when the GWGQ region is predominantly in a bent conformation, these  $i + 1$  and  $i + 2$   $\Phi$  and  $\Psi$  angles are more variable, with an average standard deviation of  $58^\circ$  (decreasing to a standard deviation of  $29^\circ$  over the shorter time spent in the H-bonded turn conformation from 45 to 48.2 ns).

### Ac-P[HGG0]GW-NH<sub>2</sub> and Ac-P[HGG1]GW-NH<sub>2</sub> simulations

The structural flexibility of the backbone region about the metal center of the HGG0 atoms is shown in two different orientations in Fig. 3, generated from 20 randomly selected time points. The RMSD of the HGG heavy atoms in Fig. 3 is  $\sim 0.21 \text{ \AA}$  at 300 K. Over the course of the full 5-ns trial simulation at 300 K, the average RMSD of the HGG heavy atoms is  $0.36 \pm 0.06 \text{ \AA}$ , with an only slightly larger variation of  $0.38 \pm 0.07 \text{ \AA}$  observed at 500 K. The 5-ns simulations demonstrate that the HGG0 and HGG1 regions are stable and are suitable for larger simulations (HGG1 data not shown).

### OR<sub>2</sub>, HGG0 topology: Ac-P[HGG0]GWGQP[HGG0]GW-NH<sub>2</sub>

A total of 10 simulations were carried out with this model system in two sets of  $5 \times 50$ -ns simulations: the first (series I) contains two dihedral angle restraints—in addition to those defining the copper-binding plane—on the histidine residue to maintain the lowest energy conformation, and the second set of simulations (series II) uses a minimal set of His dihedral angle parameters, potentially allowing for more flexibility of the  $C_\alpha$ ,  $C_\beta$ , and imidazole groups. In the second series of simulations, although the initial geometry about the metal centers is in geometry 1 (see above), the side-chain flexibility could potentially allow for interconversion between geometry 1 and geometry 2.

The RMSD plots (selected simulations are shown in Fig. 4, A and B, for series I and II, respectively) are generated relative to each simulation's starting conformation before the equilibration step, and the rise in RMSD indicates that the



FIGURE 2 Metal-free OR<sub>2</sub> structures randomly sampled over the 150-ns simulation. Their GWGQ backbone heavy atoms are aligned with the residues of the bend highlighted, shown in two 90°-rotated orientations.

structures have moved away from the starting conformation. In the course of all 10 simulations, the size of the fluctuations in the RMSD plots decreases within the first 15 ns in almost all cases, and within 25 ns in one instance. The decrease in RMSD fluctuations correlates with the formation of a stable, compact conformation in all simulations.

In all simulations, the decrease in RMSD fluctuation is accompanied by the GWGQ linker region adopting a bent conformation—as observed in the metal-free simulation (see above)—and the  $\text{Cu}^{2+}$ -binding regions collapsing together. During these simulations the GWGQ linker region forms bend-and-turn-type structures similar to those observed in the metal-free simulation. Additional turn conformations of the linker region are sampled in the  $\text{Cu}^{2+}$ -containing simulations, such as a three-residue turn involving an H-bonding interaction between the Trp-5 amide H-atom and the backbone amide O-atom of Gln-7 (residue numbers are shown in Fig. 1 C). Although this structure incorporates an H-bonding interaction, it does not fit the normal definition of a turn, as the H-bonding occurs in the reverse direction.

The bending of the linker region facilitates close approach of the HGG regions, with the planar  $\text{Cu}^{2+}$  sites forming stacked structures that interact via either their top or bottom face. No solvent molecules are present between the interacting faces of the  $\text{Cu}^{2+}$  sites in the collapsed structures, allowing the binding sites to come within the van der Waals contact range.

All 10 initial  $\text{OR}_2$  structures at time 0 begin in a fully-elongated conformation, where the  $\Phi$  and  $\Psi$  angles in the GWGQ region are approximately  $-140^\circ$  and  $135^\circ$ , respectively. In this initial conformation, both Cu atoms are maximally separated ( $\sim 22$  Å). At the same time points at which the RMSDs settle in Fig. 4, A and B, the Cu-bound HGG sites collapse and the internuclear Cu-Cu distances fall below  $\sim 7$  Å or lower, as shown in Fig. 4, C and D. Larger average internuclear Cu-Cu separations are observed in top-to-top complexes (Fig. 5 C). The top-to-top complexes are less compact and therefore give rise to larger internuclear Cu-Cu separations.

A simulation of the  $\text{OR}_2$  peptide with both of the Cu-HGG regions initially in the higher-energy conformation (geometry 2 in the DFT studies) was run (data not shown). As in the

series II simulations, a minimal number of restraints about the His residue and metal center were employed to potentially allow for interconversion between geometry 1 and geometry 2. In this instance, the local geometry does not convert to geometry 1 and the Cu centers do not approach closer than  $\sim 8.5$  Å in the course of the simulation.

### Structure of the linker region between copper-binding sites

Plots of the  $\Phi$  and  $\Psi$  angles for each of the residues in the linker region, as well as overlays of the GWGQ backbone, are shown in Fig. 6. The overlaid structures in Fig. 6, as well as each point on the  $\Phi/\Psi$  plots, are generated from 2000 snapshots over the final 20 ns of selected simulations where the specific stacking modes shown in Fig. 5 are observed. Secondary-structure analysis from all simulations shows that the GWGQ linker region between copper-binding sites has a high propensity for forming a bend, as shown for various models of stacking interactions. Even in simulations where the peptide is still essentially in an elongated conformation at time 0, the local GWGQ region frequently samples a bent conformation early on. Bending of the short GWGQ region facilitates collapse of the peptide model, allowing close approach and appropriate stacking of the copper-binding sites. These observations are analogous to the metal-free simulation shown in Fig. 2.

### Copper-copper internuclear separation

Regardless of the type of stacking between the metal binding sites, the internuclear Cu separations are generally all within the same range,  $\sim 4$ – $7$  Å (averaged from the last 20 ns of all 10 simulations, from series I and II). The bottom-to-top and top-to-bottom conformations are relatively flexible and display a wide spread of copper-copper separations in the collapsed conformations:  $5.67 \pm 0.42$  Å and  $6.15 \pm 0.44$  Å, respectively. The copper-copper separation in the top-to-top conformation is  $5.83 \pm 0.67$  Å, with both copper-binding sites interacting relatively loosely (with one metal-binding site sliding between the top face of the other copper-binding site and its adjacent Pro residue). The copper-copper distance in

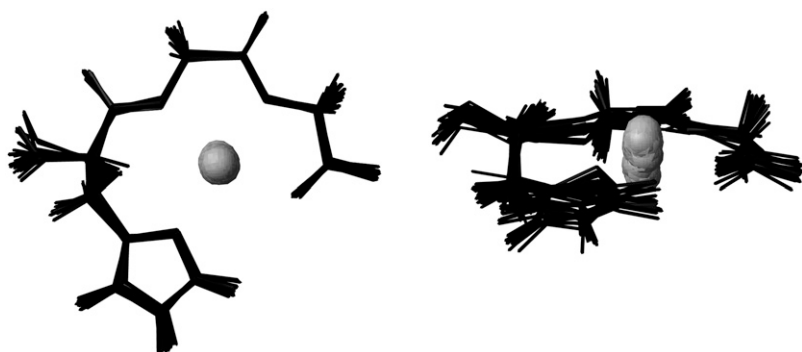
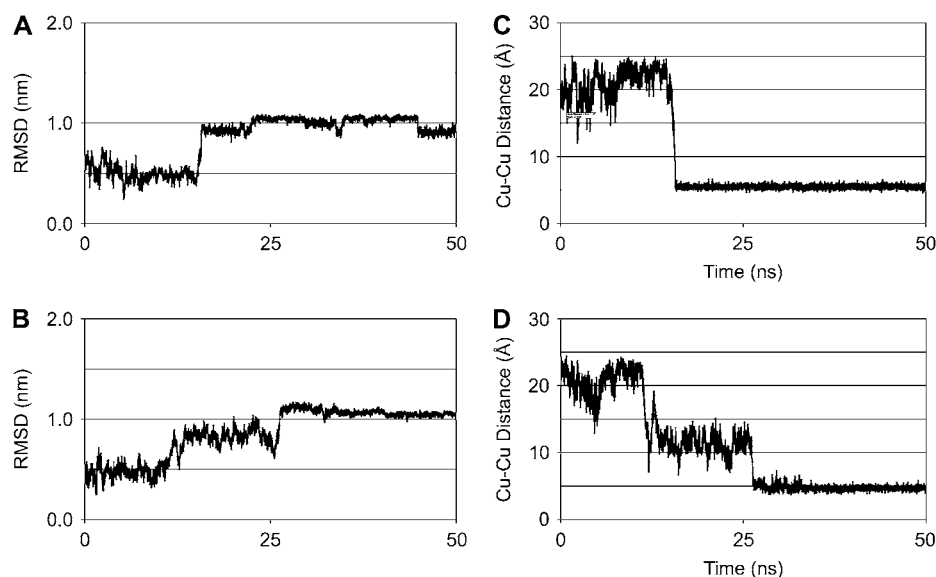


FIGURE 3 Overlay of the backbone heavy atoms from 20 randomly selected MD structures of the copper-containing HGG0 residue topology, shown in two  $90^\circ$  orientations. Flexible regions are related to allowed vibrational modes. The backbone heavy atom RMSD is  $\sim 0.21$  Å and shows that the copper-binding site is stable throughout the simulation.



**FIGURE 4** (A and B) All-atom OR<sub>2</sub> RMSD plots for representative simulations from series I (A), which uses restraints for the His side-chain conformation to maintain rigidity, and series II (B), which does not use any His side-chain dihedral restraints. RMSD plots are generated relative to a single fully extended conformation of the OR<sub>2</sub> peptide. (C and D) Internuclear Cu-Cu separation for the simulations shown in A and B, respectively. Note that the major change in the RMSD occurs at the same time as the collapse of the Cu-Cu distances; this was found in all 10 simulations (five each in series I and II).

the bottom-to-bottom conformation is  $4.96 \pm 0.32$  Å, demonstrating that this conformation is more stable and compact compared to the other stacking structures observed. No interconversion is observed between different stacking orientations on the timescales of these simulations. Only in the case of the top-to-top structure (from simulation 3 of series II, not shown) are the metal-binding sites seen to separate after initially collapsing. During this separation, the Cu-HGG sites form a transient T-shaped structure, interacting via the top face of one site and the edge of the second (the average Cu-Cu separation is  $\sim 9$  Å) before re-forming the initial top-to-top geometry.

Close approach of the copper-binding sites does not appear to be an artifact of the representation of the Cu-HGG site. The His imidazole rings of the OR<sub>2</sub> peptide also come into close proximity within the first 10 ns of the metal-free simulation. Plotting the internuclear separation between the imidazole N-atoms that would otherwise coordinate Cu<sup>2+</sup> (the N<sub>δ</sub>1-atoms), the closest approach occurs only for those conformations where the GWGQ region is bent. Of the conformations explored over the 150-ns metal-free simulation, 41% have an N<sub>δ</sub>1-N<sub>δ</sub>1 separation  $< 10$  Å, and 7% are  $< 5$  Å—with an approximately linear decrease in this proportion over the 10–5 Å range. This data is summarized in Fig. S5 in Supplementary Material.

## DISCUSSION

OPLS was employed in these simulations because it is an all-atom force field specifically designed for the purpose of modeling peptides and organic molecules in the condensed phase (51). The CHARGE charge-calculation method at the B3LYP/6-31G(d) level was used for the original parameterization of the force field and was therefore the logical choice for generating charges for the new residue topologies

described herein. The PME method for treatment of electrostatic interactions is currently regarded as a reliable method for calculating such interactions within biomolecular simulations. Comparisons between various methods, including PME, by Baumketner and Shea have shown that although the PME approach is computationally costly, it accurately reproduces the experimentally-derived free-energy minimum of test peptide models (60).

PrP is capable of responding to a range of Cu<sup>2+</sup> concentrations in its local environment at the exterior membrane surface of the synapse (43). The OR region of PrP can bind Cu<sup>2+</sup> in three distinctly different coordination modes, represented schematically in Fig. 7 A. At low [Cu<sup>2+</sup>], each OR cooperatively binds to the metal and involves a minimum of three (likely four) His imidazole side chains. This mode of binding is referred to as a 1:1 (one Cu<sup>2+</sup> ion/one OR region) coordination in Fig. 7 A. At intermediate [Cu<sup>2+</sup>], one copper bridges two ORs via two His imidazoles and a single deprotonated backbone amide N-atom, most likely from one of the coordinating His residues or its neighboring Gly—referred to as 2:1 coordination in Fig. 7 A. When the local [Cu<sup>2+</sup>] is high, each OR site can bind up to one equivalent of copper (Fig. 7 A, 4:1). These simulations are relevant to the fully-Cu<sup>2+</sup>-bound form of the OR region under conditions of high Cu<sup>2+</sup> load.

Both the metal-free and metal-bound simulations indicate that the linker region between each of the PHGG sequences in the OR region adopts a bent or turn structure—which have the same approximate shape and backbone conformation. Of the three potential copper coordination modes available to the OR region, the 4:1 form of the OR sites, modeled herein, likely induces the largest degree of structuring within the N-terminal domain of PrP.

The binding environment of the Cu<sup>2+</sup>-containing HGG models we used correspond to the equatorial N<sub>3</sub>O<sub>1</sub> donor atom environment that persists as the dominant species at

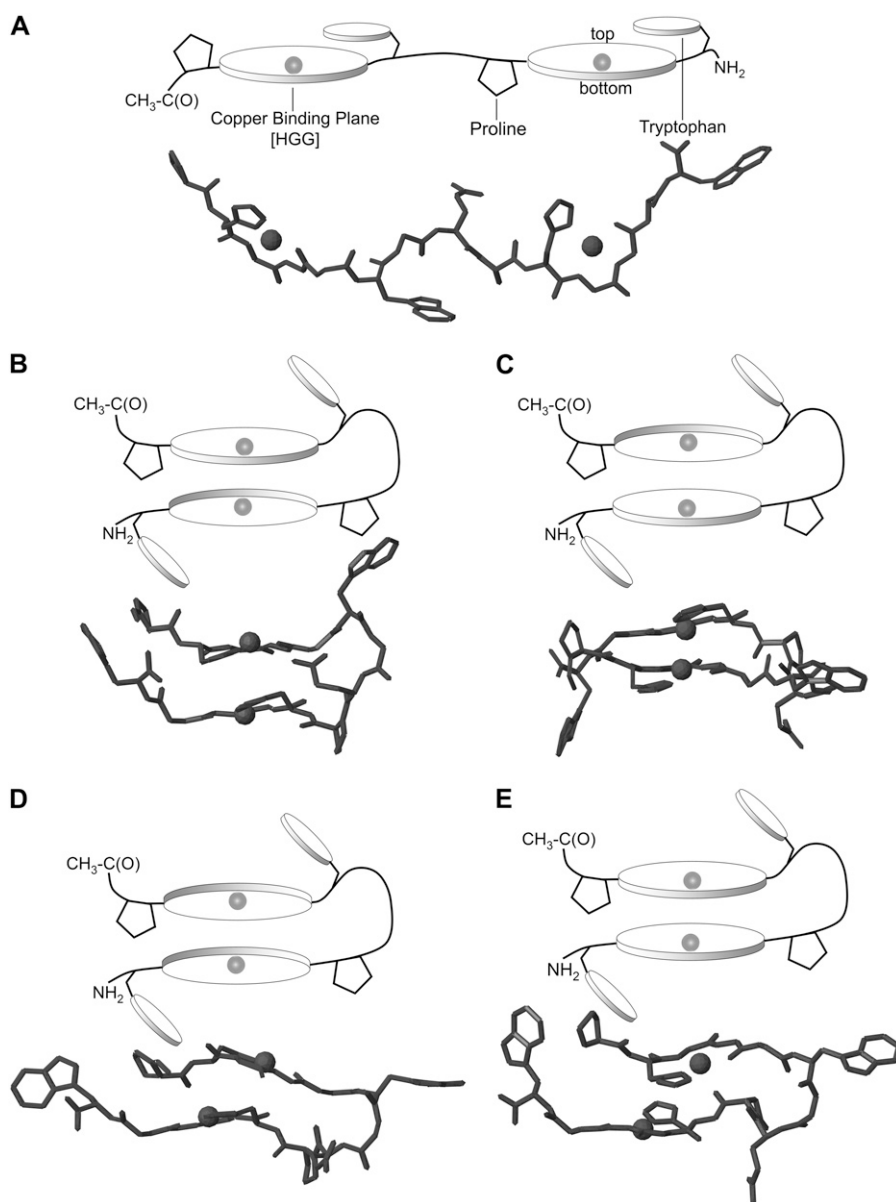


**FIGURE 5** Representations of the copper-bound OR<sub>2</sub> models. Structures shown in cartoon format are used to represent the most relevant structural features of the major conformations observed in all simulations. A single snapshot of the molecule from the simulation is shown below each. The shorthand notation used with each structure indicates which face of the first planar copper site in the sequence is interacting with which face of the second site: (A) Fully extended, with the copper-binding sites maximally separated; (B) bottom-to-bottom (*b*→*b*); (C) top-to-top (*t*→*t*); (D) top-to-bottom (*t*→*b*); and (E) bottom-to-top (*b*→*t*).

physiological pH. This is the consensus coordination mode of the fully-Cu<sup>2+</sup>-loaded octarepeat region for the cellular form of PrP, and this model is consistent with EPR, crystallographic, and x-ray absorption data (31,32,43,61). Due to the inflexibility of the peptide backbone residues at the Cu<sup>2+</sup>-binding sites, there appears to be only one relevant stable conformation for this region. Because the Cu<sup>2+</sup>-binding portions maintain only the one conformation, this significantly reduces the conformational space accessible to the OR<sub>2</sub> peptide model we used. Therefore, the bulk of the conformational flexibility in the fully-Cu<sup>2+</sup>-loaded OR region originates primarily in the linker region.

The most significant observations from the metal-free OR<sub>2</sub> simulation are that the HGG region adopts a flexible loop conformation, whereas the GWGQ linker region samples predominantly bend-and-turn-type conformations. Once

formed, the bending of the linker region persists in both the metal-free and all of the metal-bound simulations. There are a total of five GWGQ segments spanning the OR region in human PrP, each one flanking a copper-binding site (Fig. 1 A). Each of these linker regions is likely to form transient bends in the metal-free form of PrP—and may be subsequently stabilized in other copper-bound states, such as those shown in Fig. 7, B and C.

Throughout the simulations of metal-bound peptides, the copper-binding sites arrange themselves into specific orientations after the collapse of the peptide. Of the conformations explored, those of interest are observed to persist for several nanoseconds, and in some cases much longer. There are five major arrangements of copper-coordination sites observed: 1), no interaction, where both copper-binding sites are separated for some finite time, similar to the configuration in



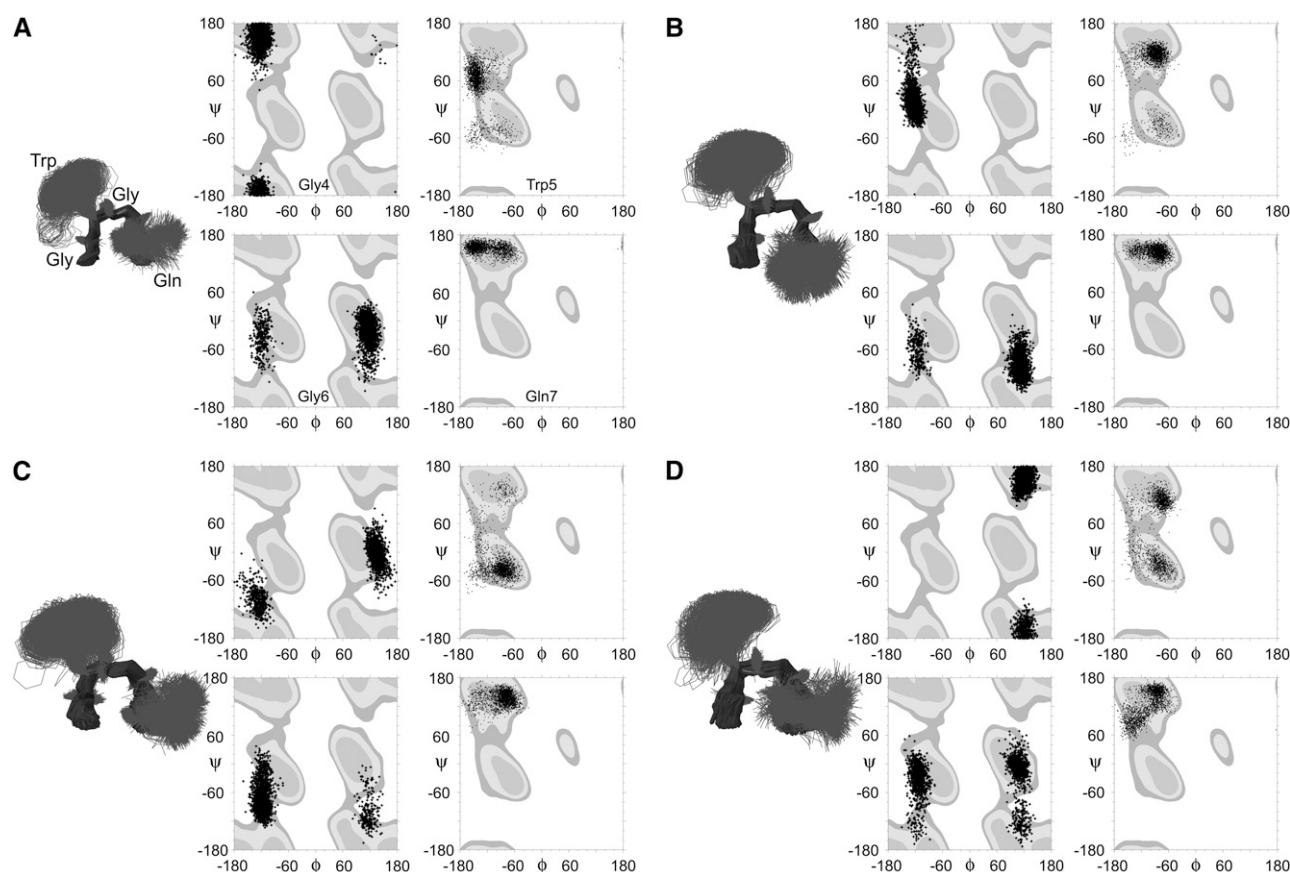


FIGURE 6 Bending of the GWQG linker region in the copper-bound OR<sub>2</sub> simulations. Overlaid structures are generated from the GWQG backbone heavy atoms and are highlighted. Each of the structures and the points on the  $\Phi/\Psi$  plots are generated from the last 20 ns of selected simulations. Distinctions are made between sets of data based on the type of copper-copper stacking arrangement observed: (A) bottom-to-bottom; (B) top-to-top; (C) top-to-bottom; and (D) bottom-to-top.

Fig. 5 A; 2), bottom-to-bottom ( $b \rightarrow b$ ) orientation, as in Fig. 5 B; 3), loosely stacked top-to-top ( $t \rightarrow t$ ) orientation, as in Fig. 5 C; 4), top-to-bottom ( $t \rightarrow b$ ) orientation, as in Fig. 5 D; or 5), bottom-to-top ( $b \rightarrow t$ ) orientation, as in Fig. 5 E. In the top-to-top case, the copper-coordination sites slide across one another, allowing the top of the second copper-binding site to also facially interact with the first proline. In addition to the major conformations, there are other transient orientations of copper-binding sites that persist for shorter durations, including side-on interaction of one copper-binding site with one face of another.

The most common structure encountered in these simulations, containing either the HGG1 (results not shown) or HGG0 topology, is the bottom-to-bottom arrangement of copper-binding structures. This arrangement is sufficiently stable that no other conformations are significantly explored within the simulation time once it is formed. In several instances, the bottom-to-bottom stacking persists for the entire 50 ns, having already been achieved during the 5-ns equilibration phase. These observations effectively put a minimum folding time limit on the formation of the stacking structures—potentially  $<5$  ns.

An EPR investigation of copper ions bound to tandem OR sites, by Chattopadhyay et al. has revealed weak diamagnetic coupling between the copper centers. Because coupling between paramagnetic centers is distance-dependent, it has been possible to derive Cu-Cu distances in the range of 3.0–6.0 Å from these experiments (43). The measured Cu-Cu distances in these simulations demonstrate that all of the copper-binding sites may lie within van der Waals contact. The copper separations indicate that each of the collapsed OR<sub>2</sub> structures (shown in Fig. 5, B–E) is compatible with the experimentally derived range of internuclear separation.

Structuring within the copper-bound OR domain has been observed elsewhere as well. The CD measurements of Garnett and Viles, using peptide fragments derived from the OR region, provide direct evidence that once Cu<sup>2+</sup> is bound to consecutive HGGGW sequences, the metal centers are not isolated from one another, and specific structuring of the linker region occurs (36). This conclusion was inferred from the CD fingerprint of the fully-Cu<sup>2+</sup>-loaded OR<sub>4</sub> peptide fragment, which contains additional elements of structure unaccounted for by the sum of the spectra for four single Cu<sup>2+</sup>-bound OR fragments alone. Yoshida et al. (39),

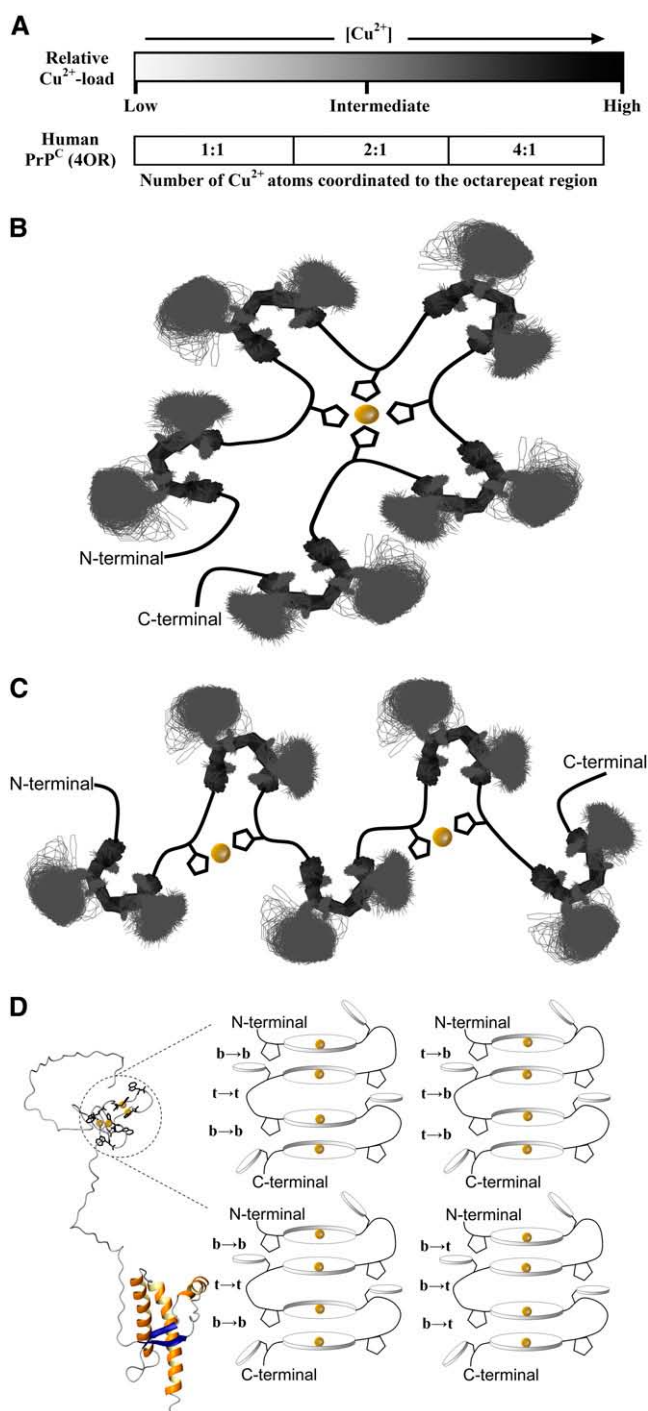


FIGURE 7 (A) The types of copper-coordination mode presented by the PrP OR region in response to the local copper concentration within the synaptic cleft. (B and C) Examples of the local backbone conformation in the OR region of PrP under various copper loads, e.g., the 4:1 complex (B) and the 2:1 complex (C), based on the conformational preference of the GWGQ residues flanking each HGG portion. (D) The observed stacking structures of the metal-bound OR<sub>2</sub> models are extended to the full-length OR<sub>4</sub> region of human PrP. Each of the stacking orientations is denoted to the left of the interacting pairs and corresponds to one of the metal-bound OR<sub>2</sub> structures observed in the MD simulations.

and Zahn (40), using peptide fragments of the OR region in the absence of  $\text{Cu}^{2+}$ , confirmed that the GWGQ region has a propensity to adopt a bent conformation, as collapse of the metal-free peptide is not apparent from their results. Data from all of the simulations carried out here indicate that this same region maintains its propensity to adopt a bent structure in the presence of bound  $\text{Cu}^{2+}$ , and that the bend of the linker region facilitates the collapse of the copper-binding sites.

Several attempts have been made to obtain information about the structure of the copper-bound OR region in solution. Łuczowski et al. (62) proposed a copper-bound structure that has some differences in the primary coordination sphere of  $\text{Cu}^{2+}$  that are not compatible with the  $\text{N}_3\text{O}_1$  coordination environment at physiological pH for the 4:1 Cu-OR complex (43). A structural study by Mentler et al. has used the apparent close association of the Trp ring NH, observed by Łuczowski et al. (62), as a distance restraint in conformational searches of  $\text{Cu}^{2+}$  bound to Ac-PHGGGWGQ-NH<sub>2</sub> in concert with a host of other experimentally derived parameters (63). Other models, offered by Bonomo et al., suggested additional coordination of adjacent backbone carbonyl O-atoms to the apical positions of the core  $\text{N}_3\text{O}_1$  complex (64). Although these structures appear to be isoenergetic with the four-coordinate  $\text{N}_3\text{O}_1$  complex (data not shown), the current lack of sufficient evidence for such interactions from NMR relaxation experiments (42) or the only available crystal structure (32) has guided us toward explicitly defining only the core  $\text{N}_3\text{O}_1$  four-coordinate complex.

The published x-ray crystal structure of the copper-bound HGGGW peptide fragment of the OR site shows the indole ring of the Trp side chain stacked above the His imidazole ring at the copper-binding site (32). Other experiments, such as <sup>1</sup>H NMR relaxation rates, give evidence for the close approach of the Trp indole to the bound  $\text{Cu}^{2+}$  center (62). The persistence of this interaction in solution is not directly evident from the experimental data and could be a transient interaction. The Trp residue has been shown, experimentally, to be necessary for structuring the binding site for  $\text{Cu}^{2+}$  within the octarepeats and directing a preferred  $\text{N}_3\text{O}_1$  donor atom count for the metal center (31). Quenching of Trp fluorescence, upon the addition of  $\text{Cu}^{2+}$ , is also often used to monitor  $\text{Cu}^{2+}$  binding to the OR domains (9). Tryptophan fluorescence quenching indicates recognition of  $\text{Cu}^{2+}$  binding by the Trp residues. The mechanism of Trp quenching has not been fully elucidated but may occur from transient conformations where the Trp makes a close approach to the paramagnetic  $\text{Cu}^{2+}$  center and bound imidazole. Such an approach would also increase the relaxation rates of those Trp indole protons closest to the metal ion.

The copper-containing HGG model topologies implemented herein are static structures, with the ligand sphere held in place. For this reason, we cannot address any dynamic structural influence that Trp may have on coordination geometry or donor atom variability of the bound

copper ion. However, during these simulations, the Trp side chains make frequent close approaches to  $\text{Cu}^{2+}$  through the exposed face of the coordination sites that are not involved in stacking interactions.

The  $\text{Cu}^{2+}$ -HGGGW crystal structure implicates a direct role for the Trp at the coordination site, through H-bonding between the indole ring and a water molecule coordinated at the metal center. Bound water molecules within the first solvation shell of aqueous  $\text{Cu}^{2+}$ , generally regarded as  $[\text{Cu}(\text{H}_2\text{O})_6]^{2+}$ , undergo rapid exchange (on the order of  $1 \times 10^9 \text{ s}^{-1}$ ) (65). Within the copper-bound OR regions, the doubly deprotonated peptide backbone makes the overall charge of the metal complex neutral. This decreased charge at the metal center will likely lead to a reduced propensity for axial water interaction with the copper center, over the  $2+$  ion. Only one coordinated water molecule is observed in the crystal structure of  $\text{Cu}^{\text{II}}(\text{Ac-HGGGW-NH}_2)_{-2\text{H}}$  (32), the frequency of solvent exchange from the apical positions is as yet unknown. Close approach ( $<6 \text{ \AA}$ ) of two adjacent Cu atoms in the HGG sites can only occur when the interacting faces of the copper-binding sites are desolvated. This realization is important in reconciling the short internuclear Cu-Cu distances observed by EPR (43) with the consensus  $\text{N}_3\text{O}_1$  coordination environment of the ORs (32,43).

Considering the bottom-to-bottom structures, the presence of additional copper-bound ORs would allow for more varied interaction between nonadjacent coppers through exchange of facially interacting coordination sites. Analysis of peptide-peptide, peptide-solvent, and solvent-solvent interaction energies indicates that there is little difference in the total energy of the system for the various stacking conformations explored. Larger  $\text{OR}_4$  simulations may yield significant energy differences between extended stacking structures, indicating which conformations may be more favored. As all of the observed stacking interactions for the dicopper-bound  $\text{OR}_2$  fragment appear to be isoenergetic, mixtures of conformations for this region may exist.

From the metal-free and metal-bound simulations, the propensity for the linker region to adopt a flexible bend is evident. Fig. 7, *B* and *C*, shows an overlay of the bent GWGQ sequence with the OR region with the 1:1 and 2:1 copper-coordination modes. Although there may be additional elements of structure within either of these coordination environments, the bend of the linker region observed herein neatly accommodates these other modes of  $\text{Cu}^{2+}$  binding as well.

Extending the structures of the model  $\text{OR}_2$  peptide to the full-length OR region in PrP yields a larger assortment of potential conformations of an  $\text{OR}_4$  fragment. Examples of the types of conformations possible for an  $\text{OR}_4$  fragment are presented in Fig. 7 *D*, and are all related to the observed  $\text{OR}_2$  conformations shown in Fig. 5. Because the backbone loops back on itself for each adjacent OR to interact, the extended  $\text{OR}_4$  domain could accommodate an extended stacking structure between adjacent ORs.

## CONCLUSIONS

The short  $\text{OR}_2$  fragments used here demonstrate the most relevant features that would be observed for larger copper-containing OR models, specifically the preferred conformations of the flexible GWGQ linker region and the potential stacking interactions of the collapsed copper-binding sites. The internuclear Cu-Cu separations obtained from these simulations are within the experimental range observed by Chattopadhyay et al., determined from EPR measurements of  $\text{Cu}^{2+}$  bound to tandem ORs (43). Renner et al. reported that the OR region can preorganize through interaction with micelles, and the structuring persists in the presence of  $\text{Cu}^{2+}$  (66). The results herein provide an additional level of structure information that may aid in refinement of OR-membrane interaction models. The CD experiments of Garnett and Viles have shown that the OR region, which is normally flexible, contains additional structure elements in the presence of  $\text{Cu}^{2+}$  (36). The results of the metal-free simulations show that the GWGQ linker region remains flexible, interconverting between a number of local bend-and-turn-type conformations, whereas the copper-bound form of the same  $\text{OR}_2$  peptide demonstrates stabilization of the bent conformation of the GWGQ region. It is clear that although the N-terminal region of PrP, as a whole, may be largely unstructured, these results demonstrate the potential for stabilization of the local structure within the fully-copper-loaded OR sequence under conditions of high  $[\text{Cu}^{2+}]$  in the prion protein's local environment. These simulations only address the potential for intrarepeat stacking of neighboring copper-binding sites; interrepeat stacking between OR regions of neighboring PrP molecules may also be possible.

After synaptic release of copper, any free copper ions that are in the  $\text{Cu}^{2+}$  oxidation state can readily participate in the generation of ROS (15). Under conditions of high  $[\text{Cu}^{2+}]$ , the 4:1 OR coordination mode binds  $\text{Cu}^{2+}$  in a redox-inactive state, protecting against the deleterious effects of potential Fenton-type or Haber-Weiss chemistry. We propose that the stacking of individual copper-binding sites in the manner presented herein may further enhance the neuroprotective mechanism of PrP by sequestering the redox-inactivated  $\text{Cu}^{2+}$  sites and limiting access by solvent or other extraneous species, which may promote ROS formation.

## SUPPLEMENTARY MATERIAL

An online supplement to this article can be found by visiting BJ Online at <http://www.biophysj.org>.

We thank Prof. D. P. Tieleman, Prof. V. Nekipelov, and Prof. A. Rauk, from the University of Calgary, for useful discussions.

This research has been enabled by the use of WestGrid computing resources, which are funded in part by the Canada Foundation for Innovation, Alberta Innovation and Science, BC Advanced Education, and the participating research institutions. This research was supported by the Canadian Genetic Diseases Network and the Alberta Agricultural Research Institute. M.J.P. is supported by an Alberta Ingenuity studentship, and

H.J.V. is the holder of a Scientist award from the Alberta Heritage Foundation for Medical Research.

## REFERENCES

- Prusiner, S. B. 1991. Molecular biology of prion diseases. *Science*. 252:1515–1522.
- Huang, Z., J. Gabriel, M. A. Baldwin, R. J. Fletterick, S. B. Prusiner, and F. E. Cohen. 1994. Proposed three-dimensional structure for the cellular prion protein. *Proc. Natl. Acad. Sci. USA*. 91:7139–7143.
- Riek, R., S. Hornemann, G. Wider, R. Glockshuber, and K. Wüthrich. 1997. NMR characterization of the full-length recombinant murine prion protein, mPrP(23–231). *FEBS Lett.* 413:282–288.
- Donne, D. G., J. H. Viles, D. Groth, I. Mehlhorn, L. J. Thomas, F. E. Cohen, S. B. Prusiner, P. E. Wright, and H. J. Dyson. 1997. Structure of the recombinant full-length hamster prion protein PrP(29–231): the N terminus is highly flexible. *Proc. Natl. Acad. Sci. USA*. 94:13452–13457.
- Pan, K., M. Baldwin, J. Nguyen, M. Gasset, A. Serban, D. Groth, I. Mehlhorn, Z. Huang, R. J. Fletterick, F. E. Cohen, and S. B. Prusiner. 1993. Conversion of  $\alpha$ -helices into  $\beta$ -sheets features in the formation of the scrapie prion proteins. *Proc. Natl. Acad. Sci. USA*. 90:10962–10966.
- Prusiner, S. B. 1982. Novel proteinaceous infectious particles cause scrapie. *Science*. 216:136–144.
- van Rheede, T., M. M. W. Smolenaars, O. Madsen, and W. W. de Jong. 2003. Molecular evolution of the mammalian prion protein. *Mol. Biol. Evol.* 20:111–121.
- Hornshaw, M. P., J. R. McDermott, and J. M. Candy. 1995. Copper binding to the N-terminal tandem repeat regions of mammalian and avian prion protein. *Biochem. Biophys. Res. Commun.* 207:621–629.
- Stöckel, J., J. Safar, A. C. Wallace, F. E. Cohen, and S. B. Prusiner. 1998. Prion protein selectively binds copper(II) ions. *Biochemistry*. 37:7185–7193.
- Viles, J. H., F. E. Cohen, S. B. Prusiner, D. B. Goodin, P. E. Wright, and H. J. Dyson. 1999. Copper binding to the prion protein: Structural implications for four identical cooperative binding sites. *Proc. Natl. Acad. Sci. USA*. 96:2042–2047.
- Kramer, M. L., H. D. Kratzin, B. Schmidt, A. Römer, I. Windl, S. Leimann, S. Hornemann, and H. Kretschmar. 2001. Prion protein binds copper within the physiological concentration range. *J. Biol. Chem.* 276:16711–16719.
- Hartter, D. E., and A. Barnea. 1988. Evidence for release of copper in the brain: depolarization-induced release of newly taken-up <sup>67</sup>copper. *Synapse*. 2:412–415.
- Vassallo, N., and J. Herms. 2003. Cellular prion protein function in copper homeostasis and redox signaling at the synapse. *J. Neurochem.* 86:538–544.
- Rae, T. D., P. J. Schmidt, R. A. Pufhal, V. C. Culotta, and T. V. O'Halloran. 1999. Undetectable intracellular free copper: the requirement of a copper chaperone for superoxide dismutase. *Science*. 284:805–808.
- Halliwell, B., and J. M. C. Gutteridge. 1984. Oxygen toxicity, oxygen radicals, transition metals and disease. *Biochem. J.* 219:1–4.
- Haber, F., and J. Weiss. 1934. The catalytic decomposition of hydrogen peroxide by iron salts. *Proc. R. Soc. Lond. A*. 147:332–351.
- Walling, C. 1982. The nature of the primary oxidants in oxidations mediated by metal ions. In *Oxidases and Related Redox Systems*. T. E. King, H. S. Mason, and M. Morrison, editors. Pergamon Press, Oxford, UK. 85–97.
- Brown, D. R., F. Hafiz, L. L. Glasssmith, B. Wong, I. M. Jones, C. Clive, and S. Haswell. 2000. Consequences of manganese replacement of copper for prion protein function and proteinase resistance. *EMBO J.* 19:1180–1186.
- Kuczius, T., A. Buschmann, W. Zhang, H. Karch, K. Becker, G. Peters, and M. H. Groschup. 2004. Cellular prion protein acquires resistance to proteolytic degradation following copper ion binding. *Biol. Chem.* 385:739–747.
- Sigurdsson, E. M., D. R. Brown, M. A. Alim, H. Scholtzova, R. Carp, H. C. Meeker, F. Prelli, B. Frangione, and T. Wisniewski. 2003. Copper chelation delays the onset of prion disease. *J. Biol. Chem.* 278:46199–46202.
- Oesch, B., D. Westaway, M. Wälchli, M. P. McKinley, S. B. Kent, R. Aebersold, R. A. Barry, P. Tempst, D. B. Teplow, L. E. Hood, S. B. Prusiner, and C. Weissmann. 1985. A cellular gene encodes scrapie PrP 27–30 protein. *Cell*. 40:735–746.
- Collinge, J., A. E. Harding, F. Owen, M. Poulter, R. Lofthouse, A. M. Boughey, T. Shah, and T. Crow. 1989. Diagnosis of Gerstmann-Sträussler syndrome in familial dementia with prion protein gene analysis. *Lancet*. ii:15–17.
- Owen, F., M. Poulter, R. Lofthouse, J. Collinge, T. J. Crow, D. Risby, H. F. Baker, R. M. Ridley, K. Hsiao, and S. B. Prusiner. 1989. Insertion in prion protein gene in familial Creutzfeldt-Jakob disease. *Lancet*. i:51–52.
- Goldfarb, L. G., P. Brown, W. R. McCombie, D. Goldgaber, G. D. Swergold, P. R. Wills, L. Cervenakova, H. Baron, C. J. Gibbs, Jr., and D. C. Gajdusek. 1991. Transmissible familial Creutzfeldt-Jakob disease associated with five, seven, and eight extra octapeptide coding repeats in the PRNP gene. *Proc. Natl. Acad. Sci. USA*. 88:10926–10930.
- van Harten, B., W. A. van Gool, I. M. van Langen, J. M. Deekman, P. H. S. Meijerink, and H. C. Weinstein. 2000. A new mutation in the prion protein gene: a patient with dementia and white matter changes. *Neurology*. 55:1055–1057.
- Flechsigs, E., D. Shmerling, I. Hegyi, A. J. Raebler, M. Fischer, A. Cozzio, C. von Mering, A. Aguzzi, and C. Weissmann. 2000. Prion protein devoid of the octapeptide repeat region restores susceptibility to scrapie in PrP knockout mice. *Neuron*. 27:399–408.
- Thackray, A. M., R. Knight, S. J. Haswell, R. Bujdoso, and D. R. Brown. 2002. Metal imbalance and compromised antioxidant function are early changes in prion disease. *Biochem. J.* 362:253–258.
- Requena, J. R., D. Groth, G. Legname, E. R. Stadtman, S. B. Prusiner, and R. L. Levine. 2001. Copper-catalyzed oxidation of the recombinant SHa(29–231) prion protein. *Proc. Natl. Acad. Sci. USA*. 98:7170–7175.
- Lovell, M. A., J. D. Robertson, W. J. Teesdale, J. L. Campbell, and W. R. Markesbery. 1998. Copper, iron and zinc in Alzheimer's disease senile plaques. *J. Neurol. Sci.* 158:47–52.
- Huang, X., C. S. Atwood, M. A. Hartshorn, M. A. Multhaup, L. E. Goldstein, R. C. Scarpa, M. P. Cuajungco, D. N. Gray, J. Lim, R. D. Moir, R. E. Tanzi, and A. I. Bush. 1999. The A $\beta$  peptide of Alzheimer's disease directly produces hydrogen peroxide through metal ion reduction. *Biochemistry*. 38:7609–7616.
- Aronoff-Spencer, E., C. S. Burns, N. I. Avdievich, G. J. Gerfen, J. Peisach, W. E. Antholine, H. L. Ball, F. E. Cohen, S. B. Prusiner, and G. L. Millhauser. 2000. Identification of the Cu<sup>2+</sup> binding sites in the N-terminal domain of the prion protein by EPR and CD spectroscopy. *Biochemistry*. 39:13760–13771.
- Burns, C. S., E. Aronoff-Spencer, C. M. Dunham, P. Lario, N. I. Avdievich, W. E. Antholine, M. M. Olmstead, A. Vrielink, G. J. Gerfin, J. Peisach, W. G. Scott, and G. L. Millhauser. 2002. Molecular features of the copper binding sites in the octarepeat domain of the prion protein. *Biochemistry*. 41:3991–4001.
- Knaus, K. J., M. Morillas, W. Swietnicki, M. Malone, W. K. Surewicz, and V. C. Yee. 2001. Crystal structure of the human prion protein reveals a mechanism for oligomerization. *Nat. Struct. Biol.* 8:770–774.
- Smith, C. J., A. F. Drake, B. A. Banfield, G. B. Bloomberg, M. S. Palmer, A. R. Clarke, and J. Collinge. 1997. Conformational properties of the prion protein octa-repeat and hydrophobic sequences. *FEBS Lett.* 405:378–384.
- Donne, D. G., J. H. Viles, D. Groth, I. Mehlhorn, T. L. James, F. E. Cohen, S. B. Prusiner, P. E. Wright, and H. J. Dyson. 1997. Structure of the recombinant full-length hamster prion protein PrP(29–231): the N-terminus is highly flexible. *Proc. Natl. Acad. Sci. USA*. 94:13452–13457.
- Garnett, A. P., and J. H. Viles. 2003. Copper binding to the octarepeats of the prion protein. Affinity, specificity, folding, and cooperativity: insights from circular dichroism. *J. Biol. Chem.* 278:6795–6802.

37. Riek, R., S. Hornemann, G. Wider, R. Glockshuber, and K. Wüthrich. 1997. NMR characterization of the full-length recombinant murine prion protein, mPrP(23–231). *FEBS Lett.* 413:282–288.
38. Zahn, R., A. Liu, T. Luhrs, R. Riek, C. von Schroetter, F. Lopez-Garcia, M. Billeter, L. Calzolari, G. Wider, and K. Wüthrich. 2000. NMR solution structure of the human prion protein. *Proc. Natl. Acad. Sci. USA.* 97:145–150.
39. Yoshida, H., N. Matsushima, Y. Kumaki, M. Nakata, and K. Hikichi. 2000. NMR studies of model peptides of PHGGGWGQ repeats within the N-terminus of prion proteins: a loop conformation with histidine and tryptophan in close proximity. *J. Biochem. (Tokyo).* 128:271–281.
40. Zahn, R. 2003. The octapeptide repeats in mammalian prion protein constitute a pH-dependent folding and aggregation site. *J. Mol. Biol.* 334:477–488.
41. Gustiananda, M., J. R. Liggins, P. L. Cummins, and J. E. Gready. 2004. Conformation of prion protein repeat peptides by FRET measurements and molecular dynamics simulations. *Biophys. J.* 86:2467–2483.
42. Pushie, M. J., and A. Rauk. 2003. Computational studies of Cu(II)[peptide] binding motifs: Cu[HGGG] and Cu[HG] as models for Cu(II) binding to the prion protein octarepeat region. *J. Biol. Inorg. Chem.* 8:53–65.
43. Chattopadhyay, M., E. D. Walter, D. J. Newell, P. J. Jackson, E. Aronoff-Spencer, J. Peisach, G. J. Gerfen, B. Bennett, W. E. Antholine, and G. L. Millhauser. 2005. The octarepeat domain of the prion protein binds Cu(II) with three distinct coordination modes at pH 7.4. *J. Am. Chem. Soc.* 127:12647–12656.
44. Becke, A. D. 1993. Density-functional thermochemistry. III. The role of exact exchange. *J. Chem. Phys.* 98:5648–5652.
45. Frisch, M. J., Trucks, G. W., Schlegel, H. B., Scuseria, G. E., Robb, M. A., Cheeseman, J. R., Montgomery, Jr., J. A., Vreven, T., Kudin, K. N., Burant, J. C., Millam, J. M., Iyengar, S. S., Tomasi, J., Barone, V., Mennucci, B., Cossi, M., Scalmani, G., Rega, N., Petersson, G. A., Nakatsuji, H., Hada, M., Ehara, M., Toyota, K., Fukuda, R., Hasegawa, J., Ishida, M., Nakajima, T., Honda, Y., Kitao, O., Nakai, H., Klene, M., Li, X., Knox, J. E., Hratchian, H. P., Cross, J. B., Bakken, V., Adamo, C., Jaramillo, J., Gomperts, R., Stratmann, R. E., Yazyev, O., Austin, A. J., Cammi, R., Pomelli, C., Ochterski, J. W., Ayala, P. Y., Morokuma, K., Voth, G. A., Salvador, P., Dannenberg, J. J., Zakrzewski, V. G., Dapprich, S., Daniels, A. D., Strain, M. C., Farkas, O., Malick, D. K., Rabuck, A. D., Raghavachari, K., Foresman, J. B., Ortiz, J. V., Cui, Q., Baboul, A. G., Clifford, S., Cioslowski, J., Stefanov, B. B., Liu, G., Liashenko, A., Piskorz, P., Komaromi, I., Martin, R. L., Fox, D. J., Keith, T., Al-Laham, M. A., Peng, C. Y., Nanayakkara, A., Challacombe, M., Gill, P. M. W., Johnson, B., Chen, W., Wong, M. W., Gonzalez, C., and Pople, J. A. 2004. Gaussian 03, Revision C.02. Gaussian, Wallingford, CT.
46. Barone, V., and M. Cossi. 1998. Quantum calculation of molecular energies and energy gradients in solution by a conductor solvent model. *J. Phys. Chem. A.* 102:1995–2001.
47. Cossi, M., N. Rega, G. Scalmani, and V. Barone. 2003. Energies, structures, and electronic properties of molecules in solution with the C-PCM solvation model. *J. Comput. Chem.* 24:669–681.
48. Carlson, H. A., T. B. Nguyen, M. Orozco, and W. L. Jorgensen. 1993. Accuracy of free energies of hydration for organic molecules from 6–31G\*-derived partial charges. *J. Comput. Chem.* 10:1240–1249.
49. Berendsen, H. J. C., D. van der Spoel, and R. van Drunen. 1995. GROMACS: A message-passing parallel molecular dynamics implementation. *Comput. Phys. Commun.* 91:43–56.
50. Lindahl, E., B. Hess, and D. van der Spoel. 2001. GROMACS 3.0: a package for molecular simulation and trajectory analysis. *J. Mol. Model.* 7:306–317.
51. Jorgensen, W. L., D. S. Maxwell, and J. Tirado-Rives. 1996. Development and testing of the OPLS all-atom force field on conformational energetics and properties of organic liquids. *J. Am. Chem. Soc.* 118:11225–11236.
52. Berendsen, H. J. C., J. P. M. Postma, A. DiNola, and J. R. Haak. 1984. Molecular dynamics with coupling to an external bath. *J. Chem. Phys.* 81:3684–3690.
53. Essman, U., L. Perela, M. L. Berkowitz, T. Darden, H. Lee, and L. G. Pedersen. 1995. A smooth particle mesh Ewald method. *J. Chem. Phys.* 103:8577–8592.
54. Miyamoto, S., and P. A. Kollman. 1992. SETTLE: an analytical version of the SHAKE and RATTLE algorithms for rigid water models. *J. Comput. Chem.* 13:952–962.
55. Hess, B., H. Bekker, H. J. C. Berendsen, and J. G. E. M. Fraaije. 1997. LINCS: a linear constraint solver for molecular simulations. *J. Comput. Chem.* 18:1463–1472.
56. Kabsch, W., and C. Sander. 1983. Dictionary of protein secondary structures: pattern recognition of hydrogen-bonded and geometrical features. *Biopolymers.* 22:2577–2637.
57. Humphrey, W., A. Dalke, and K. Schulten. 1996. VMD: visual molecular dynamics. *J. Mol. Graph.* 14:33–38.
58. Koradi, R., M. Billeter, and K. Wüthrich. 1996. MOLMOL: a program for display and analysis of macromolecular structures. *J. Mol. Graph.* 14:51–55.
59. Daura, X., K. Gademann, B. Jaun, B. Seebach, W. F. van Gunsteren, and A. E. Mark. 1999. Peptide folding: when simulation meets experiment. *Angew. Chem. Int. Ed.* 38:236–240.
60. Baumketner, A., and J. Shea. 2005. The influence of different treatments of electrostatic interactions on the thermodynamics of folding of peptides. *J. Phys. Chem. B.* 109:21322–21328.
61. Morante, S., R. González-Iglesias, C. Potrich, C. Meneghini, W. Meyer-Klaucke, G. Menestrina, and M. Gasset. 2004. Inter- and intra-octarepeat Cu(II) site geometries in the prion protein: implications in Cu(II) binding cooperativity and Cu(II)-mediated assemblies. *J. Biol. Chem.* 279:11753–11759.
62. Łuczowski, M., H. Kozłowski, M. Stawikowski, M. Rolka, E. Gaggelli, D. Valensin, and G. Valensin. 2002. Is the monomeric prion octapeptide repeat PHGGGWGQ a specific ligand for Cu<sup>2+</sup> ions? *J. Chem. Soc., Dalton Trans.* 2269–2274.
63. Mentler, M., A. Weiss, K. Grantner, P. del Pino, D. Deluca, S. Fiori, C. Renner, W. M. Klaucke, L. Moroder, U. Bertsch, H. A. Kretschmar, P. Tavan, and F. G. Parak. 2005. A new method to determine the structure of the metal environment in metalloproteins: investigation of the prion protein octapeptide repeat Cu<sup>2+</sup> complex. *Eur. Biophys. J.* 34:97–112.
64. Bonomo, R. P., V. Cucinotta, A. Giuffrida, G. Impellizzeri, A. Magri, G. Pappalardo, E. Rizzarelli, A. M. Santoro, G. Tabbi, and L. I. Vagliasindi. 2005. A re-investigation of copper coordination in the octa-repeats region of the prion protein. *J. Chem. Soc., Dalton Trans.* 150–158.
65. Lippard, S. J., and J. M. Berg. 1994 *Principles of Bioinorganic Chemistry*. University Science Books, Mill Valley, CA, pp 29.
66. Renner, C., S. Fiori, F. Fiorino, D. Landgraf, D. Deluca, M. Mentler, K. Grantner, F. G. Parak, H. Kretschmar, and L. Moroder. 2004. Micellar environments induce structuring of the N-terminal tail of the prion protein. *Biopolymers.* 73:421–433.